

# High-Dimensional Carrier-Assisted Entanglement Purification Based on Mutually Unbiased Bases

Zihua Song<sup>1</sup>, Lin Chen<sup>\*1</sup>, and Yongge Wang<sup>\*1</sup>

<sup>1</sup>LMIB(Beihang University), Ministry of Education, and School of Mathematical Sciences, Beihang University, Beijing 100191, China

May 21, 2026

## Abstract

Distilling high-dimensional quantum entanglement under realistic, general asymmetric noise remains a formidable challenge. Standard entanglement purification protocols inevitably fail to satisfy convergence constraints under severe asymmetric noise. In this paper, we investigate carrier-assisted entanglement purification protocols, namely CAEPP and mCAEPP, for two-qutrit systems, demonstrating that without adaptive pre-processing, convergence is strictly bottlenecked by marginal  $X$ -error probabilities. To overcome this limitation, we introduce a deterministic pre-processing scheme based on mutually unbiased bases (MUBs). By actively rotating the qutrit phase space to establish primary-axis error dominance, we rigorously prove that the MUB-adapted mCAEPP deterministically yields unit asymptotic fidelity for any two-qutrit Pauli channel with initial fidelity  $p_{00} > 1/3$ .

Keywords: entanglement purification; qutrit; asymmetric noise; mutually unbiased bases.

## 1 Introduction

Entanglement distillation, the extraction of pure entangled states from mixed ensembles, is a fundamental prerequisite for reliable quantum information processing [1, 2]. While the basic distillability of bipartite systems has been extensively mapped out via the positive partial transpose (PPT) and reduction criteria [3–7], characterizing and distilling full-rank mixed states under general noise remains notoriously difficult [8]. Traditionally, standard local twirling operations have been employed to convert bipartite states into highly symmetric

---

\*Corresponding authors: lichen@buaa.edu.cn (Lin Chen); wangyongge@buaa.edu.cn (Yongge Wang)

forms, such as Werner states [9], to simplify the collective processing of multiple copies [10–12]. However, to circumvent severe mathematical complexities, much of this foundational effort was strictly limited to systems with low matrix rank [13–16], alongside various quantitative estimations mostly confined to low-dimensional protocols [17–21].

Driven by the need to transcend these low-rank assumptions, high-dimensional quantum entanglement has attracted immense attention due to its enhanced information capacity and inherent resilience against noise, as systematically reviewed in [22]. State-of-the-art experimental advancements, ranging from high-dimensional quantum teleportation [23] to heralded photon-photon quantum gates [24], prove that complex multi-level coherent manipulations are now technologically viable. Despite these structural advantages, distilling high-dimensional systems under realistic, general asymmetric noise remains a formidable challenge. Investigations into the fundamental limits of quantum distillation reveal severe theoretical bottlenecks. Specifically, recent no-go theorems for universal entanglement purification [25] and catalysis-assisted distillation [26] rigorously demonstrate that standard purification protocols are fundamentally limited. Since no single, universal protocol can efficiently distill entanglement across all arbitrary noise models, conventional recurrence methods inevitably fail to satisfy the convergence constraints when confronted with severe environmental noise asymmetry. This critical bottleneck, further compounded by the complexities of high-dimensional state certification [27] and symmetric projection constraints [28], is particularly evident in entanglement-based communication under high noise [29].

Overcoming these strict theoretical and practical limitations necessitates a departure from traditional symmetric distillation. Specifically, an adaptive pre-processing strategy based on mutually unbiased bases (MUBs) is urgently required. By actively rotating the discrete phase space to secure a primary-axis error dominance, one can strictly bound the lateral errors and guarantee deterministic convergence, effectively bypassing the no-go limitations of static protocols in practical, asymmetric environments.

In this paper, we focus on the design, analysis, and extension of entanglement purification protocols in three-dimensional (qutrit) systems subject to general asymmetric noise. The remainder of this paper is organized as follows. In Section 2, we establish the theoretical framework by introducing qutrit Pauli channels, Bell-diagonal states, and entanglement fidelity. Specifically, Lemma 1 establishes that an initial fidelity  $F(\rho) > 1/3$  guarantees the state is non-entanglement-breaking and 1-distillable, setting the fundamental theoretical threshold for our protocols. Section 3 details the single-carrier-assisted entanglement purification protocol (CAEPP). Through rigorous error propagation analysis, Proposition 2 demonstrates that without adaptive pre-processing, the protocol’s convergence is strictly bottlenecked by the marginal  $X$ -error probabilities. This analytically proves that standard protocols fail under highly asymmetric noise, highlighting the necessity for an adaptive pre-processing strategy. To overcome this limitation, Section 4 introduces the multi-carrier generalized protocol (mCAEPP) via stabilizer codes. Lemmas 3 and 4 formulate the al-

gebraic properties of the bilateral encoding operations, formally dictating the syndrome extraction rules. Building on this framework, Theorem 5 proves that the mCAEPP deterministically converges to unit fidelity for symmetric depolarizing channels. To tackle general asymmetric noise, we introduce a deterministic pre-processing scheme based on MUBs. Governed by the discrete geometric properties of the qutrit phase space established in Lemma 7, this step actively rotates the phase space to enforce a primary-axis error dominance. Ultimately, our main theoretical result, Theorem 8, proves that for any two-qutrit Pauli channel with  $p_{00} > 1/3$ , the mCAEPP with adaptive MUB pre-processing deterministically purifies the shared state to unit asymptotic fidelity.

## 2 Preliminaries

To characterize three-dimensional bipartite systems and generalized Pauli channels, we first introduce the set of single-qutrit generalized Pauli operators. This set is constructed from the cyclic-shift operator  $X$  and the phase-shift operator  $Z$ , whose actions on the computational basis are defined as  $X|j\rangle = |(j+1) \bmod 3\rangle$  and  $Z|j\rangle = \omega^j|j\rangle$ , respectively, with  $\omega = e^{2\pi i/3}$ . These operators satisfy the fundamental commutation relation  $XZ = \omega ZX$ . Consequently, any operator within this set can be uniquely expressed in the form  $X^u Z^v$  for  $u, v \in \{0, 1, 2\}$ .

The fundamental resources for our protocol are the nine three-dimensional Bell states i.e., maximally entangled qutrit pairs. They form a complete orthonormal basis and are uniformly defined as

$$|\Phi^{n,m}\rangle = \frac{1}{\sqrt{3}} \sum_{j=0}^2 \omega^{mj} |j, (j+n) \bmod 3\rangle, \quad (1)$$

where  $n, m \in \{0, 1, 2\}$  represent the shift and phase indices, respectively. Notably, applying an arbitrary local Pauli operation  $I \otimes X^u Z^v$  to  $|\Phi^{n,m}\rangle$  deterministically shifts its indices, enabling mutual conversions among all nine orthogonal states up to a global phase factor.

Any three-dimensional bipartite Bell-diagonal state can be written as

$$\rho = \sum_{n,m=0}^2 p_{nm} |\Phi^{n,m}\rangle \langle \Phi^{n,m}|, \quad (2)$$

where  $\sum_{n,m=0}^2 p_{nm} = 1$ .

A three-dimensional Pauli channel  $\mathcal{N}$  is parameterized by these probabilities  $p_{nm}$  as

$$\mathcal{N}(\cdot) = \sum_{n,m=0}^2 p_{nm} Z^m X^n (\cdot) X^{-n} Z^{-m}. \quad (3)$$

When Alice sends one qutrit of  $|\Phi^{0,0}\rangle$  through  $\mathcal{N}$ , the resulting shared state, known as the CJ state of the channel, is given by

$$\sigma = (I_d \otimes \mathcal{N})\Phi^{0,0} = \sum_{n,m=0}^2 p_{nm} |\Phi^{n,m}\rangle \langle \Phi^{n,m}|. \quad (4)$$

The entanglement fidelity for three-dimensional states  $\rho$  is defined as

$$F(\rho) = \langle \Phi^{0,0} | \rho | \Phi^{0,0} \rangle = p_{00}. \quad (5)$$

The following lemma is a direct consequence of the results in [30].

**Lemma 1** *An  $N$ -dimensional channel  $\mathcal{N}$  is EB only if its corresponding CJ state  $\rho$  has an entanglement fidelity  $F(\rho) \leq 1/N$ . Furthermore, for  $N = 2$ , a Pauli channel  $\mathcal{N}$  is EB if and only if  $F(\rho) \leq 1/2$ .*

In contrast, if  $F(\rho) = p_{00} > 1/N$  then (2) violates the reduction criterion, indicating that (2) is NPT entangled and 1-distillable.

Based on these preliminaries, we first present the single-carrier CAEPP protocol in Section 3, followed by the multi-carrier generalization and stabilizer code implementation in Section 4.

### 3 Single-Carrier Assisted Entanglement Purification in three dimension

We now detail the single-carrier CAEPP protocol for two-qutrit entanglement purification.

#### 3.1 Protocol Overview

The three-dimensional CAEPP follows the core framework of two-dimension CAEPP but adapts to qutrit operations.

1. Initialization: Alice and Bob share a three-dimensional Bell-diagonal state  $\rho$  with fidelity  $F = p_{00} > 1/3$ , characterizing a non-EB channel as given by (5).

2. Pre-processing: Alice and Bob apply local unitaries to the shared pair to minimize the occurrence of pure phase errors, ensuring that the probabilities  $p_{01}$  and  $p_{02}$  are the two smallest among the nine Bell states.

3. Encoding: Alice prepares a single carrier qutrit in the initial state  $|0\rangle$ . Then she applies a three-dimensional CNOT gate  $U_{CN}$ , using her shared qutrit as the control and the carrier as the target. Following this encoding step, she transmits the carrier through the quantum channel.

4. Decoding: When receiving the carrier, Bob applies a reverse CNOT gate  $U_{CN'}$ , using his shared qutrit as the control and the carrier as the target. Subsequently, the carrier is measured in the  $Z$ -basis.

5. Decision: Alice and Bob retain the purified shared state if the syndrome measurement yields 0, indicating no detected error; otherwise, the state is discarded and the protocol restarts.

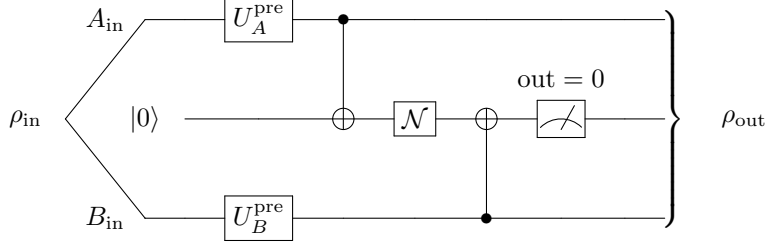


Figure 1: Quantum circuit of the single-carrier CAEPP protocol

**Notation Description:**

- $A_{\text{in}}$ : Input qutrit of the shared entangled pair at Alice's side
- $B_{\text{in}}$ : Input qutrit of the shared entangled pair at Bob's side
- $\rho_{\text{in}}$ : Initial noisy shared Bell-diagonal entangled state
- $|0\rangle$ : Initial carrier qutrit
- $U_A^{\text{pre}}, U_B^{\text{pre}}$ : Local pre-processing unitary operations
- $\mathcal{N}$ : Noisy quantum channel for shared state transmission
- $\text{out} = 0$ : Success condition of Z-basis measurement on the shared state
- $\rho_{\text{out}}$ : Purified output entangled state after successful protocol

### 3.2 Detailed Protocol Design

We now evaluate how the protocol affects the shared state  $\sigma$  in (4). Linearity permits an independent analysis of each Bell-diagonal component  $|\Phi^{n,m}\rangle \langle \Phi^{n,m}|$ . The derivation proceeds as follows.

Specifically, the action of the three-dimensional CNOT gate  $U_{CN}$  is defined as

$$U_{CN} |j\rangle_C \otimes |k\rangle_T = |j\rangle_C \otimes |(j+k) \bmod 3\rangle_T, \quad (6)$$

where the subscripts  $C$  and  $T$  denote the control and target qutrits, respectively.

Before the gate application, the joint state of the shared Bell pair and the initial carrier is

$$|\Phi^{n,m}\rangle_{AB} \otimes |0\rangle_T = \frac{1}{\sqrt{3}} \sum_{j=0}^2 \omega^{mj} |j\rangle_A \otimes |(j+n) \bmod 3\rangle_B \otimes |0\rangle_T. \quad (7)$$

In our protocol, Alice's qutrit  $A$  serves as the control and the ancillary carrier  $T$  acts as the target, while Bob's qutrit  $B$  remains unaffected as a spectator.

Applying  $U_{CN}$  between Alice's qutrit  $A$  and the carrier  $T$  transforms the target state from  $|0\rangle_T$  to  $|(j+0) \bmod 3\rangle_T = |j\rangle_T$ , yielding the joint state

$$U_{CN} (|\Phi^{n,m}\rangle_{AB} \otimes |0\rangle_T) = \frac{1}{\sqrt{3}} \sum_{j=0}^2 \omega^{mj} |j\rangle_A \otimes |(j+n) \bmod 3\rangle_B \otimes |j\rangle_T. \quad (8)$$

The carrier  $T$  is then transmitted through the quantum channel to Bob. Upon receiving it, Bob applies a reverse CNOT gate  $U_{CN'}$  using his qutrit  $B$  as the control and the carrier  $T$  as the target. The action of  $U_{CN'}$  is defined by

$$U_{CN'} |j\rangle_B \otimes |k\rangle_T = |j\rangle_B \otimes |(k-j) \bmod 3\rangle_T. \quad (9)$$

Applying  $U_{CN'}$  to the joint state yields the final pre-measurement state

$$\frac{1}{\sqrt{3}} \sum_{j=0}^2 \omega^{mj} |j\rangle_A \otimes |(j+n) \bmod 3\rangle_B \otimes |(3-n) \bmod 3\rangle_T. \quad (10)$$

Finally, Bob measures the carrier in the  $Z$ -basis and classically communicates the outcome to Alice. If the measurement yields 0, the protocol succeeds and they retain the shared pair; otherwise, they declare failure and discard the state.

### 3.3 Two-Round Purification over Noiseless Channels

Consider the ideal scenario where the ancillary carrier is transmitted through a noiseless channel with  $\mathcal{N} = I$ . Upon successful post-selection in the first round of the CAEPP, all  $X$ -errors with  $n \in \{1, 2\}$  are deterministically filtered out. The shared state thus reduces to

$$\rho_{\text{out}} = \sum_{m=0}^2 p'_{0m} |\Phi^{0,m}\rangle \langle \Phi^{0,m}|, \quad (11)$$

with the normalized probabilities given by

$$p'_{0m} = \frac{p_{0m}}{\sum_{j=0}^2 p_{0j}}. \quad (12)$$

Because this intermediate state contains only pure phase errors, executing a second round of the CAEPP in the conjugate basis achieves complete purification. Consequently, two successful rounds of the CAEPP with noiseless carriers are sufficient to deterministically distill a maximally entangled qutrit pair, referred to as an eprit, from an initially noisy shared state.

Figure 2 illustrates the corresponding quantum circuit. In Round 1, the initial qutrits  $A_{\text{in}}$  and  $B_{\text{in}}$  undergo pre-processing operations  $U_A^{\text{pre1}}$  and  $U_B^{\text{pre1}}$ , and interact with the first carrier initialized in state  $|0\rangle_1$ , yielding the partially purified state  $\rho_{\text{out}}$  upon a successful measurement outcome of  $\text{out}_1 = 0$ . Round 2 applies the subsequent pre-processing operations  $U_A^{\text{pre2}}$  and  $U_B^{\text{pre2}}$ , and utilizes the second carrier initialized in state  $|0\rangle_2$ . Upon the second successful measurement outcome of  $\text{out}_2 = 0$ , the protocol deterministically outputs the perfectly purified entangled state  $\Phi^+$ .

### 3.4 Robustness under Noisy Carriers

We now evaluate the CAEPP under practical conditions where the single-qutrit carrier is subjected to noise. Motivated by realistic communication setups, we

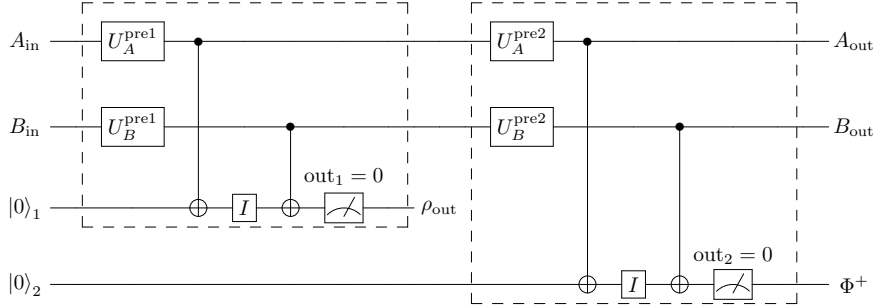


Figure 2: Quantum circuit for two-round purification over noiseless channels

**Notation Description:**

- $A_{\text{in}}, B_{\text{in}}$ : Input qutrits of the initial noisy state shared between Alice and Bob.
- $|0\rangle_1, |0\rangle_2$ : Initial states of the carrier states.
- $U_A^{\text{pre}k}, U_B^{\text{pre}k}$ : Pre-processing unitaries for Round  $k$ .
- $I$ : Noiseless quantum channel for shared state transmission.
- $\text{out}_k = 0$ : Success condition of  $Z$ -basis measurement on the shared state for Round  $k$ .
- $\rho_{\text{out}}$ : Partially purified state on shared states after Round 1 success.
- $\Phi^+$ : The final perfectly purified entangled state shared between Alice and Bob.

assume the ancillary carrier traverses the same noisy channel  $\mathcal{N}$  used to distribute the initial shared state. This scenario is mathematically modeled as two independent uses of the identical channel, represented by  $\mathcal{N} \otimes \mathcal{N}$ .

During initialization, Alice transmits one qutrit of a maximally entangled pair through  $\mathcal{N}$ , yielding the shared Bell-diagonal state defined in (4). While successful rounds of the CAEPP strictly increase the fidelity of the shared state, the presence of carrier noise generally prevents the exact distillation of a perfect eutrit. To quantify this fundamental operational limit, we define

$$F_\star := \text{the maximum convergent fidelity} \quad (13)$$

attainable through successive repetitions of the CAEPP.

### 3.5 Single-Carrier Protocol under Asymmetric Noise

We define the mixed error operator  $Y = ZX$  through the cyclic-shift operator  $X$  and the phase-shift operator  $Z$ ,

$$X |j\rangle = |(j+1) \bmod 3\rangle, \quad (14)$$

$$Z |j\rangle = \omega^j |j\rangle, \quad (15)$$

$$Y |j\rangle = ZX |j\rangle = \omega^{j+1} |(j+1) \bmod 3\rangle. \quad (16)$$

Then (3) can be rewritten as

$$\begin{aligned}
\mathcal{N}(\cdot) = & p_{00}(\cdot) + p_{01}Z(\cdot)Z^{-1} + p_{02}Z^2(\cdot)Z^{-2} \\
& + p_{10}X(\cdot)X^{-1} + p_{20}X^2(\cdot)X^{-2} \\
& + p_{11}Y(\cdot)Y^{-1} + p_{22}Y^2(\cdot)Y^{-2} \\
& + p_{12}ZY(\cdot)Y^{-1}Z^{-1} + p_{21}Z^2Y^2(\cdot)Y^{-2}Z^{-2}.
\end{aligned} \tag{17}$$

As discussed in Section 3.2, a single round of testing cannot eliminate pure  $Z$ -errors with  $n = 0$ . Consequently, we restrict our analysis to Pauli channels characterized by exactly seven non-zero probabilities by setting  $p_{01} = p_{02} = 0$ . Letting the initial fidelity be  $F_0 = p_{00}$ , this configuration can be parameterized as

$$(p_{00}, 0, 0, p_{10}, p_{11}, p_{12}, p_{20}, p_{21}, p_{22}) \tag{18}$$

where  $\sum_{n=1}^2 \sum_{m=0}^2 p_{nm} = 1 - p_{00}$ .

We now evaluate the asymptotic performance of the single-carrier protocol in the absence of pre-processing, establishing its fundamental convergence threshold in the following proposition.

**Proposition 2** *Consider a two-qutrit state transmitted with initial fidelity  $p_{00}$  and error probabilities  $p_{nm}$ , where  $p_{01} = p_{02} = 0$ . In the absence of any pre-processing, the fidelity  $F_N$  after  $N$  successful rounds of the single-carrier protocol converges to 1 as  $N \rightarrow \infty$  if and only if*

$$p_{00} > \max\{p_{10} + p_{11} + p_{12}, p_{20} + p_{21} + p_{22}\}. \tag{19}$$

**Proof.** For  $i \in \{1, 2\}$ , suppose the shared state has an error with  $n = i$  and  $m = j$ , which occurs with probability  $p_{ij}$ . To survive the final measurement, the ancillary carrier must independently acquire an error with the identical shift index  $n = i$ . This occurs with the marginal  $X$ -error probability  $p_{X=i} := \sum_{m=0}^2 p_{im}$ . Let  $P_i$  denote the probability that the protocol succeeds with a residual shift error  $n = i$ . The error-free branch requires both the shared state and the ancillary carrier to independently remain flawless, yielding  $P_0 = p_{00}^2$ .

For error branches  $i \in \{1, 2\}$ , survival dictates that the ancillary carrier must independently acquire a shift error  $n = i$  identical to that of the shared state. Defining the marginal  $X$ -error probability as  $p_{X=i} := \sum_{m=0}^2 p_{im}$ , and summing over all possible initial phase errors  $j$ , we obtain,

$$P_i = \sum_{j=0}^2 p_{ij} p_{X=i} = p_{X=i}^2. \tag{20}$$

The post-selection fidelity  $F_1$  is then simply the conditional probability,

$$F_1 = \frac{P_0}{P_0 + P_1 + P_2} = \frac{p_{00}^2}{p_{00}^2 + p_{X=1}^2 + p_{X=2}^2}. \tag{21}$$



To evaluate the fidelity  $F_2$  after the second round of CAEPP, we first express the residual error probabilities  $p'_{nm}$  generated from the first round for  $n \in \{1, 2\}$  and  $m \in \{0, 1, 2\}$  as

$$p'_{nm} = \frac{\sum_{j=0}^2 p_{n,j} p_{n,(m-j) \bmod 3}}{p_{00}^2 + p_{X=1}^2 + p_{X=2}^2}. \quad (22)$$

In the second round, the protocol operates exclusively on the purified state obtained from the first round, assisted by a new ancillary carrier traversing the identical original channel. The updated fidelity is then given by

$$F_2 = \frac{p'_{00} p_{00}}{p'_{00} p_{00} + \sum_{n=1}^2 \left( \sum_{m=0}^2 p'_{nm} \right) p_{X=n}}. \quad (23)$$

Substituting (21) and (22) into (23) and performing the algebraic simplification, the fidelity after the second round compactly becomes

$$F_2 = \frac{p_{00}^3}{p_{00}^3 + p_{X=1}^3 + p_{X=2}^3}. \quad (24)$$

By mathematical induction, this analytical structure generalizes to the  $N$ -th round. The fidelity  $F_N$  can then be directly expressed as

$$F_N = \frac{p_{00}^{N+1}}{p_{00}^{N+1} + p_{X=1}^{N+1} + p_{X=2}^{N+1}} = \left[ 1 + \left( \frac{p_{X=1}}{p_{00}} \right)^{N+1} + \left( \frac{p_{X=2}}{p_{00}} \right)^{N+1} \right]^{-1}. \quad (25)$$

To guarantee an asymptotic convergence of  $\lim_{N \rightarrow \infty} F_N = 1$ , the exponential bases in the denominator must be strictly less than 1, yielding the fundamental algebraic constraint

$$p_{00} > \max\{p_{X=1}, p_{X=2}\}. \quad (26)$$

□

This exposes a critical vulnerability to noise asymmetry. Under perfectly symmetric depolarizing noise with  $p_{X=1} = p_{X=2}$ , the protocol successfully recovers the standard threshold  $p_{00} > 1/3$  as shown in Figures 3 and 4. However, even slight noise asymmetry can violate this condition despite  $p_{00} > 1/3$ , causing the divergence illustrated in Figure 5. In the highly asymmetric limit, such as  $p_{X=1} \rightarrow 1 - p_{00}$ , the threshold drastically deteriorates, requiring  $p_{00} > 1/2$  to guarantee convergence as demonstrated in Figure 6.

Consequently, MUB pre-processing becomes a mathematical imperative. By actively rotating the phase space to upper-bound lateral error probabilities, MUB secures the universal  $p_{00} > 1/3$  convergence threshold regardless of initial asymmetry. We will explicitly introduce this MUB operation to improve the protocol in Section 4.4.

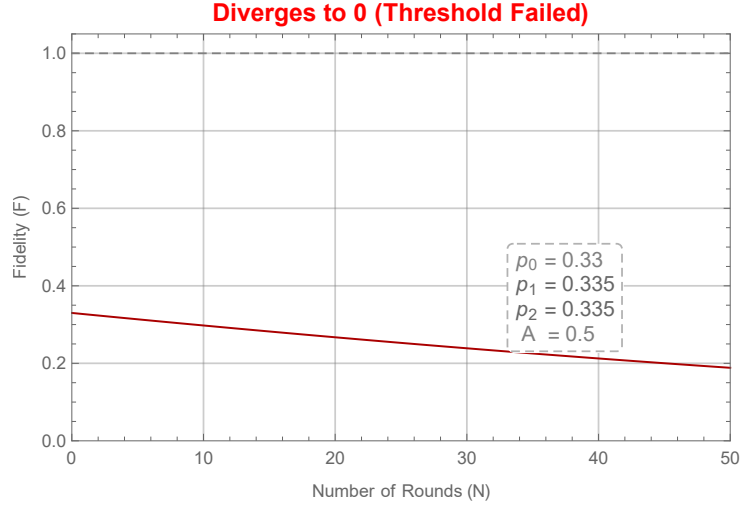


Figure 3: Asymptotic fidelity  $F_N$  of the single-carrier CAEPP without pre-processing. Inset parameters:  $p_0 := p_{00}$ ,  $p_{1,2} := p_{X=1,2}$  and  $A := p_1/(p_1 + p_2)$ . For symmetric noise with  $A = 0.5$ ,  $p_0 = 0.33$ , and  $p_1 = p_2 = 0.335$ , the convergence threshold  $p_0 > \max\{p_1, p_2\}$  is violated, causing the fidelity to strictly diverge to 0.

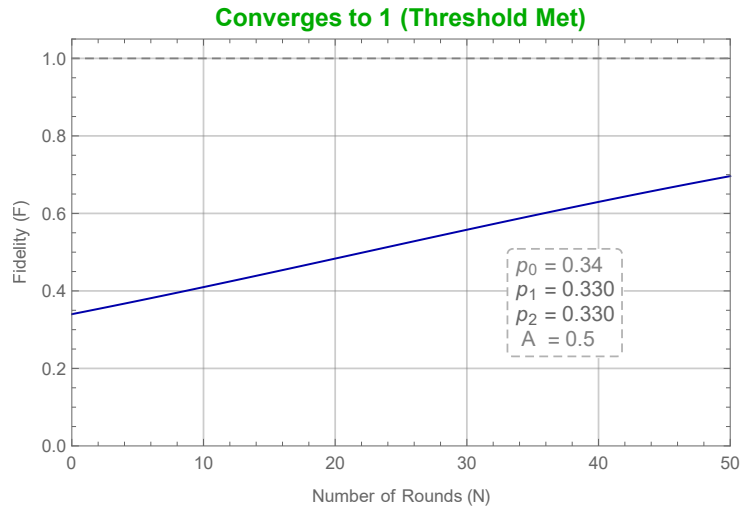


Figure 4: Asymptotic fidelity  $F_N$  without pre-processing. For symmetric noise with  $A = 0.5$ ,  $p_0 = 0.34$ , and  $p_1 = p_2 = 0.330$ , the threshold condition  $p_0 > \max\{p_1, p_2\}$  is satisfied, enabling the fidelity to asymptotically converge to 1.

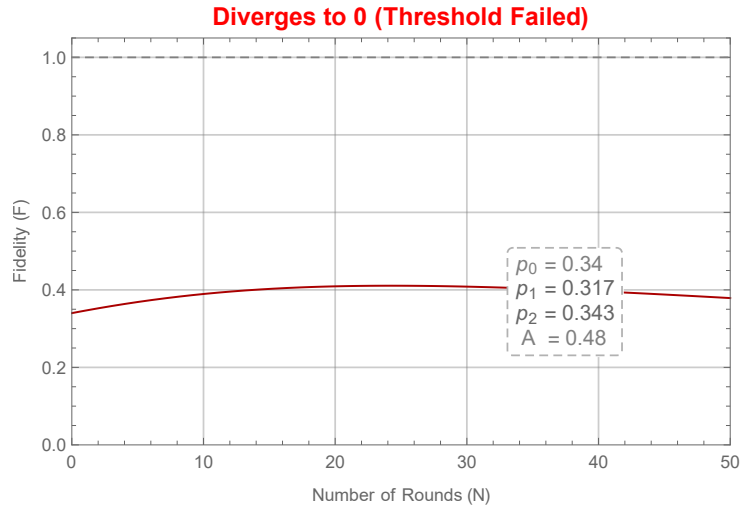


Figure 5: Asymptotic fidelity  $F_N$  without pre-processing. Under slightly asymmetric noise with  $A = 0.48$  and the same initial  $p_0 = 0.34$ , the marginal errors shift to  $p_1 = 0.317$  and  $p_2 = 0.343$ . The threshold condition  $p_0 > \max\{p_1, p_2\}$  is consequently violated, causing the fidelity to ultimately diverge to 0 despite  $p_0 > 1/3$ .

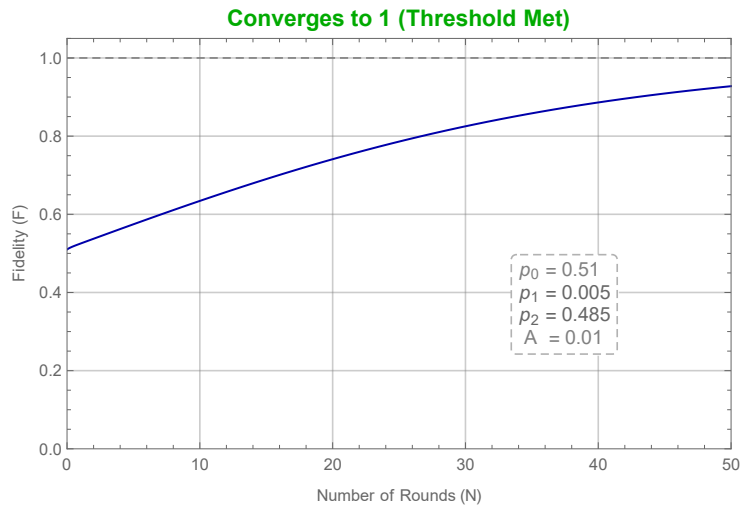


Figure 6: Asymptotic fidelity  $F_N$  without pre-processing. Under highly asymmetric noise with  $A = 0.01$  and  $p_0 = 0.51$ , the marginal errors are  $p_1 = 0.005$  and  $p_2 = 0.485$ . The threshold condition  $p_0 > \max\{p_1, p_2\}$  is satisfied, enabling the fidelity to asymptotically converge to 1.

## 4 Multi-Carrier Extensions and Stabilizer Code Implementations

Building on the single-carrier assisted entanglement purification protocol proposed in Section 3, we further generalize it to a multi-carrier scenario, yielding the mCAEPP. The core objective of this chapter is to establish the general framework of mCAEPP, which purifies a single-copy shared state to an ebit through noisy channels. This generalization is motivated by the practical demand for enhancing the robustness and scalability of purification protocols, as single-carrier systems are prone to performance degradation under severe channel noise. By leveraging the redundancy of multiple qutrit carriers, mCAEPP is capable of suppressing noise interference more effectively, thus improving the purification fidelity and success probability compared to its single-carrier counterpart. In the following sections, we will elaborate on the stabilizer code implementation, encoding/decoding operations, and a specific two-carrier case study, based on the general framework introduced here.

### 4.1 Stabilizer Code for Qutrit Purification

The purification protocol with multiple carriers can be constructed with the stabilizer code, specified by a commuting set of Pauli generators

$$S_i \in \{I_d, Z^k, X^l, Z^k X^l\}, \quad k, l \in \{1, 2\}. \quad (27)$$

In each round, Alice prepares  $m$  carrier qutrits in the code space defined by  $\{S_i\}$  and transmits them through the Pauli channel  $\mathcal{N}$ . Upon reception, Bob applies the corresponding decoding operation and measures the carriers in the  $Z$ -basis.

Environmental noise during transmission induces quantum state alterations, which are mathematically characterized by the generalized qutrit Pauli operators  $X$ ,  $Y$ , and  $Z$ . In the stabilizer formalism, a Pauli error  $E$  is detected if it anticommutes with at least one generator  $S_i$ , i.e.,  $ES_i = \omega^k S_i E$ ,  $k \bmod 3 \neq 0$  for some  $i$ . Errors commuting with all generators pass the stabilizer check and remain undetected.

### 4.2 Encoding and Decoding Operations

All scenarios discussed in this section are based on the three-dimensional case, i.e., qutrits. The carrier qutrits are initially prepared as  $|0\rangle^m$ , which is a code state of the stabilizer generators

$$\{Z_1, Z_2, \dots, Z_m\}. \quad (28)$$

In this notation,  $Z_i$  denotes the phase-shift operator  $Z = \text{diag}\{1, \omega, \omega^2\}$  acting exclusively on the  $i$ -th subsystem. The identity operator  $I_3$  is implicitly applied to the remaining subsystems.

Here the code state is a common eigenvector of (28). Specifically, the single-qutrit basis state  $|0\rangle$  is an eigenstate of the phase-shift operator  $Z$  with eigenvalue 1. Consequently, the tensor product state  $|0\rangle^{\otimes m}$  remains invariant under the action of any local operator  $Z_i$ , making it a simultaneous eigenstate of the entire stabilizer group with eigenvalue 1.

For a generator set  $\{S_i\}$ , there exists a unitary  $U_{enc}$  such that

$$U_{enc}Z_iU_{enc}^\dagger = S_i \quad \forall i \in \{1, 2, \dots, m\}. \quad (29)$$

The unitary  $U_{enc}$  is precisely an encoding operation, while  $U_{dec} = U_{enc}^\dagger$  serves as a decoding operation in the mCAEPP.

**Lemma 3** *The three-dimensional CNOT gate  $U_{CN}$  satisfies*

$$U_{CN}(I_3 \otimes Z)U_{CN}^\dagger = Z^2 \otimes Z. \quad (30)$$

**Proof.** We take the three-dimensional computational basis vectors  $|j, k\rangle$ , where  $j$  denotes the target qutrit state and  $k$  denotes the carrier qutrit state. One can verify that both the left-hand side and the right-hand side exhibit consistent action effects,

$$\begin{aligned} U_{CN}(I_3 \otimes Z)U_{CN}^\dagger |j, k\rangle &= U_{CN}(I_3 \otimes Z)(U_{CN}^\dagger |j, k\rangle) \\ &= U_{CN}(|j\rangle \otimes Z|k - j \pmod{3}\rangle) \\ &= \omega^{k-j} |j, k\rangle, \end{aligned}$$

$$Z^2 \otimes Z |j, k\rangle = Z^{-1} \otimes Z |j, k\rangle = \omega^{k-j} |j, k\rangle.$$

Since the left-hand side  $U_{CN}(I_3 \otimes Z)U_{CN}^\dagger$  and the right-hand side  $Z^2 \otimes Z$  yield equivalent effects when acting on all basis vectors  $|j, k\rangle$ , the formula holds strictly.  $\square$

**Lemma 4** *The multi-carrier encoding operator is a  $(m+1)$ -qutrit gate involving the target qutrit and  $m$  carrier qutrits, and has the form*

$$U_{CN}^m = U_{CN}^{(1)} \circ U_{CN}^{(2)} \circ \dots \circ U_{CN}^{(m)}, \quad (31)$$

where  $U_{CN}^{(i)} |j, k_1, k_2, \dots, k_m\rangle = |j, k_1, \dots, (j + k_i) \pmod{3}, \dots, k_m\rangle$ . Then we have a generalized formula,

$$U_{CN}^m(I_3 \otimes \bigotimes_{i=1}^m Z_i)(U_{CN}^m)^\dagger = Z^2 \otimes \bigotimes_{i=1}^m Z_i. \quad (32)$$

**Proof.** The proof proceeds analogously to that of Lemma 3.  $\square$

### 4.3 Case Study: Two-Carrier Instance

To specifically illustrate the working mechanism of the three-dimensional mCAEPP, we design a two-carrier qutrit protocol with  $m = 2$ . Within this framework, we select the stabilizer generators

$$\{X_1X_2^2, Z_0Z_1Z_2\}. \quad (33)$$

Here,  $X_i$  denotes the cyclic-shift operator  $X = \begin{pmatrix} 0 & 0 & 1 \\ 1 & 0 & 0 \\ 0 & 1 & 0 \end{pmatrix}$  acting on the  $i$ -th subsystem. The identity operator  $I_3$  is implicitly applied to all other subsystems within the  $m$ -body composite system.

For these operators to form a valid stabilizer group, they must commute mutually. This is readily verified by explicitly calculating their product,

$$X_1X_2^2Z_0Z_1Z_2 = \omega \cdot \omega^2Z_0Z_1Z_2X_1X_2^2 = Z_0Z_1Z_2X_1X_2^2. \quad (34)$$

Having established their commutativity, we now proceed to evaluate their error detection capabilities.

The generator  $S_1 = X_1X_2^2$  precisely detects single-carrier  $Z$ - and  $Y$ -type errors. The anti-commutation relations are explicitly given by

$$Z_1S_1 = \omega S_1Z_1, \quad (35)$$

$$Z_2S_1 = \omega^2 S_1Z_2. \quad (36)$$

Given that  $Y = XZ$ , the detection signature of  $Y$ -errors is mathematically equivalent to that of pure  $Z$ -errors.

The generator  $S_2 = Z_0Z_1Z_2$  identifies any error configuration where the total number  $k$  of  $X$ - or  $Y$ -type errors yields  $k \not\equiv 0 \pmod{3}$ . The corresponding anti-commutation relations generating the non-trivial phases are

$$X_iS_2 = \omega S_2X_i, \quad i \in \{0, 1, 2\}, \quad (37)$$

$$X_kX_lS_2 = \omega^2 S_2X_kX_l, \quad k, l \in \{0, 1, 2\}, k \neq l. \quad (38)$$

### 4.4 Scalability: Beyond Two Carriers

A larger per-round carrier number  $m$  yields a higher maximum convergent fidelity  $F_*$  and better purification performance. For non-entanglement-breaking noisy channels, the mCAEPP is capable of achieving perfect distillation with  $F_* = 1$  given a sufficient number of carriers. Specifically, we define the "star" stabilizer generators for  $m$  carriers as

$$\{X_1X_m^2, X_2X_m^2, \dots, X_{m-1}X_m^2, Z_0Z_1 \cdots Z_m\}. \quad (39)$$

By employing this stabilizer configuration, physically realized by the sequential bilateral operations depicted in Figure 7, the protocol demonstrates robust scalability against depolarizing noise, which we formalize in the following theorem.

**Theorem 5** *For a qutrit depolarizing channel with initial fidelity  $p_{00} > 1/3$ , the mCAEPP deterministically purifies the shared state to unit asymptotic fidelity.*

**Proof.** The rigorous proof relies on mapping the error propagation of the protocol to a discrete dynamical system. By employing modulo-3 indicator functions and their characteristic functions to evaluate the stabilizer constraints, we derive the exact transition probabilities for the Bell-diagonal state. This framework reveals that the survival probabilities of all non-target error branches decay exponentially with the number of carriers. By analyzing the fixed points of this dynamical map in the asymptotic limit, we systematically demonstrate that all error probabilities strictly vanish, deterministically driving the target state fidelity to unity. The complete algebraic derivation is detailed in [Appendix A](#).  $\square$

**Remark 6** *While local twirling routinely simplifies qubit Pauli channels into symmetric depolarizing ones, applying this to qutrits is fundamentally hindered by their asymmetric algebraic structure. Forced symmetrization risks degrading a distillable NPT state into an undistillable bound entangled state. This limitation prevents the direct generalization of twirling techniques, thereby necessitating our adaptive pre-processing scheme.*

## 4.5 Adaptive Pre-processing for General Pauli Channels

In traditional two-dimensional systems, local twirling operations are routinely employed to convert general Pauli channels into depolarizing channels, thereby simplifying theoretical analyses. However, directly applying this twirling technique to three-dimensional systems fundamentally alters the underlying channel structure. Because the qutrit Pauli group possesses a more complex asymmetric algebraic structure, forced symmetrization over its eight non-trivial errors inadvertently discards useful asymmetric coherent information. More critically, such twirling can transform a distillable entangled state into an undistillable bound entangled state. To address this, we bypass the twirling approximation and directly exploit the intrinsic asymmetry of the general qutrit Pauli noise.

The core idea of our scheme hinges on establishing a strictly dominant error direction in the phase space. To achieve this without discarding coherent information, we bypass the twirling approximation and exploit the geometric structure of three-dimensional MUBs. The feasibility of this adaptive pre-processing is guaranteed by the following geometric property of the qutrit discrete phase space.

**Lemma 7** *Let  $p_{nm}$  denote the probabilities of a two-qutrit Bell-diagonal state on the discrete phase space  $\mathbb{Z}_3 \times \mathbb{Z}_3$ , and let  $L_1, \dots, L_4$  be the sum of probabilities associated with the four MUBs. If  $p_{00} > 1/3$ , the maximum among these  $L_i$  satisfies  $L_{\max} := \max\{L_1, \dots, L_4\} > 1/2$ .*

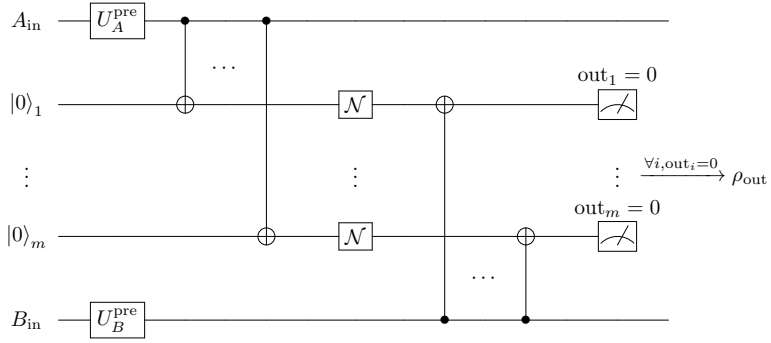


Figure 7: Quantum circuit for the scalable generalized mCAEPP with  $m$  carriers.

**Notation Description:**

- $A_{\text{in}}, B_{\text{in}}$ : Input qutrits of the initial noisy state shared between Alice and Bob.
- $|0\rangle_1, \dots, |0\rangle_m$ : Initial states of the carrier states.
- $U_A^{\text{pre}}, U_B^{\text{pre}}$ : Local pre-processing unitaries applied by Alice and Bob.
- **CNOTs**: Sequential collective encoding by Alice and star-stabilizer syndrome extraction by Bob.
- $\mathcal{N}$ : The identical qutrit depolarizing channel acting independently on each carrier.
- $\text{out}_i = 0$ : The post-selection success condition requiring all  $m$  syndrome measurements to yield 0.
- $\rho_{\text{out}}$ : The deterministically purified output state, which asymptotically approaches unit fidelity as  $m$  increases.



**Proof.** In prime dimension  $d = 3$ , the  $d + 1 = 4$  MUBs correspond to four independent directional axes in the discrete phase space. These four lines, all intersecting exclusively at the origin  $(0, 0)$ , completely partition the eight non-origin lattice points without overlap.

The sums of probabilities associated with these four bases, specifically the  $Z$ ,  $X$ ,  $XZ$ , and  $XZ^2$  bases, are given by

$$\begin{aligned} L_1 &= p_{00} + p_{10} + p_{20}, \\ L_2 &= p_{00} + p_{01} + p_{02}, \\ L_3 &= p_{00} + p_{11} + p_{22}, \\ L_4 &= p_{00} + p_{12} + p_{21}. \end{aligned} \tag{40}$$

Because these four directional lines share only the origin state, summing them counts  $p_{00}$  four times while counting every other error probability  $p_{nm}$  exactly once. Therefore, the total sum evaluates to

$$\sum_{i=1}^4 L_i = 3p_{00} + \sum_{n,m=0}^2 p_{nm} = 3p_{00} + 1. \tag{41}$$

Given the initial fidelity threshold  $p_{00} > 1/3$ , it rigorously follows that  $\sum_{i=1}^4 L_i > 2$ . By the pigeonhole principle, at least one of the four sums must strictly exceed  $1/2$ , yielding  $L_{\max} > 1/2$ .  $\square$

Lemma 7 provides a deterministic target for our adaptive pre-processing. By applying bilateral local Clifford operations, Alice and Bob align the maximum-error MUB axis  $L_{\max}$  with the primary  $Z$ -basis  $L_1$ . This targeted basis transformation deterministically forces the lateral  $X$ -error probabilities to satisfy  $\max\{p_{X=1}, p_{X=2}\} < 1/2$ , rigidly fulfilling the necessary convergence constraint. Once this primary-axis dominance is secured, the complete adaptive protocol illustrated in Figure 8 exponentially suppresses all lateral error branches through joint post-selection, culminating in our main theoretical result.

**Theorem 8** *For any two-qutrit Pauli channel with initial fidelity  $p_{00} > 1/3$ , the mCAEPP with adaptive MUB pre-processing deterministically purifies the shared state to unit asymptotic fidelity.*

The detailed asymptotic convergence proof for Theorem 8 is provided in [Appendix B](#).

## 5 Conclusion

We established a deterministic entanglement distillation framework for three-dimensional systems under general asymmetric Pauli noise. As demonstrated, single-carrier purification strictly diverges under severe noise asymmetry. To resolve this, we introduced the mCAEPP utilizing stabilizer codes and an adaptive pre-processing strategy based on MUBs. By rotating the discrete phase

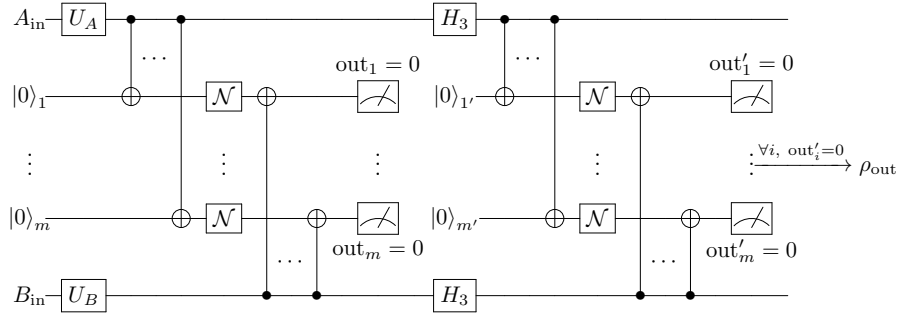


Figure 8: Quantum circuit of the adaptive mCAEPP. Local Clifford gates  $U_A$  and  $U_B$  pre-align the maximum-error MUB axis  $L_{\max}$  with the primary  $Z$ -basis  $L_1$ , followed by alternating-basis measurements.

**Notation Description:**

- $A_{\text{in}}, B_{\text{in}}$ : Input qutrits of the noisy shared state.
- $|0\rangle_i, |0\rangle_{i'}$ : Initial states of the  $m$  carriers for the two alternating-basis rounds.
- $U_A, U_B$ : Adaptive MUB pre-processing unitaries from the local Clifford group, such as the Hadamard gate  $H_3$ .
- **CNOTs**: Bilateral SUM gates for sequential collective encoding by Alice and syndrome extraction by Bob.
- $H_3$ : Qutrit Hadamard gate applied bilaterally to toggle between  $X$ - and  $Z$ -errors.
- $\mathcal{N}$ : The independent qutrit Pauli noisy channel acting on each carrier.
- $\text{out}_i = 0, \text{out}'_i = 0$ : Syndrome measurement success conditions.
- $\rho_{\text{out}}$ : The conditionally purified state retained upon successful post-selection.

space to align the maximum-error MUB axis with the primary quantization basis, this strategy enforces a primary-axis error dominance. Consequently, for any two-qutrit Pauli channel with an initial fidelity strictly greater than  $1/3$ , the mCAEPP deterministically suppresses all errors, achieving unit asymptotic fidelity.

While this protocol provides a robust framework for high-dimensional quantum communication networks, several problems remain for future investigation. First, generalizing the MUB-based geometric rotation from  $d = 3$  to arbitrary dimensions  $d > 3$  requires addressing the increasingly complex structures of generalized Pauli groups. Second, the asymptotic performance of the mCAEPP under continuous non-Pauli noise models requires further theoretical modeling and potential adaptations of syndrome extraction rules. Finally, the  $1/3$  theoretical threshold assumes flawless local operations. Developing a fault-tolerant analysis to bound the tolerable local gate infidelity during pre-processing and parity checks is necessary for practical experimental implementations.

## Acknowledgements

ZHS and LC were supported by the NNSF of China (Grant No. 12471427).

## Appendix A Discussion of 4.4

Let the shared state after Round  $n$  be a Bell-diagonal state (2) with probabilities

$$q^{(n)} = (q_{00}, q_{01}, q_{02}, q_{10}, q_{11}, q_{12}, q_{20}, q_{21}, q_{22}). \quad (42)$$

At the Pre-processing step, Alice and Bob apply local unitaries to the shared pair, which rearranges the probabilities to

$$\begin{aligned} \mathbf{r} &= (r_{00}, r_{01}, r_{02}, r_{10}, r_{11}, r_{12}, r_{20}, r_{21}, r_{22}) \\ &= (q_{00}, q_{21}, q_{22}, q_{10}, q_{11}, q_{12}, q_{20}, q_{01}, q_{02}). \end{aligned} \quad (43)$$

The errors affecting the shared state and the  $m$  carriers during transmission can be represented by a  $(2m + 2)$ -bit error string

$$E = E_0 \otimes E_1 \otimes \cdots \otimes E_m, \quad (44)$$

where  $E_0 = Z^{z_0} X^{x_0}$  is the error of the shared state and  $E_i = Z^{z_i} X^{x_i}$  is the error of the  $i$ -th carrier.

For  $S_i = X_i X_m^2$ ,  $i = 1, \dots, m - 1$  in (39),  $ES_i = S_i E$  holds provided that the following condition is satisfied,

$$\omega^{z_i + 2z_m} = \omega^0, \quad (45)$$

$$\Leftrightarrow z_i + 2z_m \equiv 0 \pmod{3}, \quad (46)$$

$$\Leftrightarrow z_i = z_m \pmod{3}. \quad (47)$$

For  $S_m = Z_0 Z_1 \cdots Z_m$ ,  $ES_m = S_m E$  holds provided that the following condition is satisfied,

$$\omega^{\sum_{j=0}^m x_j} = \omega^0 \Leftrightarrow \sum_{j=0}^m x_j \equiv 0 \pmod{3}. \quad (48)$$

To sum up, the general conditions for the success of the purification protocol are as follows,

$$\begin{cases} z_i = z_m \pmod{3}, i = 1, 2, \dots, m-1. \\ \sum_{j=0}^m x_j \equiv 0 \pmod{3}. \end{cases} \quad (49)$$

Since we design the shared state and the carriers to pass through the same channel—which, in this context, corresponds to the depolarizing channel with  $p := p_{00}$  (See the top of page 30). The probability for the carriers is thus obtained.

The error probabilities of carrier qutrits are distributed as

$$P_k(i, j) := P(x_k = i, z_k = j) = \begin{cases} p, & (i, j) = (0, 0), \\ \frac{1-p}{8}, & (i, j) = \text{else}, \end{cases} \quad (50)$$

where  $k = 1, 2, \dots, m$  and

$$P_0(i, j) := P(x_0 = i, z_0 = j) = r_{ij}. \quad (51)$$

We assume that the shared state has stabilized after the  $n$ -th round of the protocol. This implies that the state probabilities are invariant under an additional round, and that the output state coincides with the input state after any round. Subsequent calculations rely on the equality among the state probabilities after the  $(n+1)$ -th round, those after the  $n$ -th round, and the corresponding steady-state probabilities.

To evaluate the success probability  $P_{\text{succ}}$  and the probabilities  $\mathbf{q}'$  characterizing the shared state after Round  $n+1$ ,

$$\mathbf{q}' := \mathbf{q}^{(n+1)} = (q'_{00}, q'_{01}, q'_{02}, q'_{10}, q'_{11}, q'_{12}, q'_{20}, q'_{21}, q'_{22}), \quad (52)$$

we introduce a success indicator  $\mathbf{1}_{\text{succ}}$  defined over the error strings specified in (44). This indicator takes the value 1 if the round ends in **Success**, and 0 otherwise.

We can now proceed to construct the three-dimensional success indicator  $\mathbf{1}_{\text{succ}}$  by (49),

$$\mathbf{1}_{\text{succ}} = \left( \prod_{i=1}^{m-1} \delta_0(z_i - z_m) \right) \cdot \delta_0(x_0 + x_1 + \cdots + x_m). \quad (53)$$

Afterwards, based on the properties of the indicator function, to calculate the probability of protocol success, we only need to compute the expectation of  $\mathbf{1}_{\text{succ}}$ ,

$$P_{\text{succ}} = \mathbb{E}[\mathbf{1}_{\text{succ}}] = P\left( \bigcap_{i=1}^{m-1} \{z_i = z_m \pmod{3}\} \cap \left\{ \sum_{k=0}^m x_k \equiv 0 \pmod{3} \right\} \right). \quad (54)$$

We will calculate  $P_{\text{succ}}$  in the following steps.

- (i) Variable distribution analysis;
- (ii) Decomposition of the total probability formula;
- (iii) Simplify the expression;
- (iv) Calculate each part separately;
- (v) Calculate  $P_{\text{succ}}$ .

Here is the first step.

- (i) Variable distribution analysis.

Let  $\{(x_k, z_k)\}$  be a sequence of independent and identically distributed (i.i.d.) random pairs, where each component takes values in  $\{0, 1, 2\}$ , i.e.,  $x_k, z_k \in \{0, 1, 2\}$ . Their joint probability mass function (pmf) is given by

$$P_k(i, j) = \begin{cases} p, & (i, j) = (0, 0), \\ \frac{1-p}{8}, & (i, j) = \text{else.} \end{cases} \quad (55)$$

We refer to the marginal pmf as the sum of the joint pmf over all possible values of another random variable.

The marginal pmf of  $z_k$  for  $c \in \{0, 1, 2\}$  is

$$C_c := P(z_k = c) = \sum_{i=0}^2 P_k(i, c) = \begin{cases} \frac{3p+1}{8}, & c = 0 \\ \frac{3(1-p)}{8}, & c = 1, 2 \end{cases} \quad (56)$$

and the marginal pmf of  $x_k$  for  $t \in \{0, 1, 2\}$  is

$$T_t := P(x_k = t) = \sum_{j=0}^2 P_k(t, j) = \begin{cases} \frac{3p+1}{8}, & t = 0 \\ \frac{3(1-p)}{8}, & t = 1, 2 \end{cases} \quad (57)$$

Let the conditional pmf  $r_c(t) = P(x_k = t | z_k = c)$  for  $c, t \in \{0, 1, 2\}$ , then

$$r_c(t) = \begin{cases} r_0(t) = \begin{cases} \frac{4p}{3p+1}, \\ \frac{1-p}{2(3p+1)}, \\ \frac{1-p}{2(3p+1)}, \end{cases} \\ r_1(t) = \frac{1}{3}, \quad t \in \{0, 1, 2\}, \\ r_2(t) = \frac{1}{3}, \quad t \in \{0, 1, 2\}. \end{cases} \quad (58)$$

(ii) Decomposition of the total probability formula.

$$P_{\text{succ}} = P\left(\bigcap_{i=1}^{m-1} \{z_i = z_m \pmod{3}\} \cap \left\{\sum_{k=0}^m x_k \equiv 0 \pmod{3}\right\}\right) \quad (59)$$

$$= \sum_{c=0}^2 \left( \prod_{j=1}^m P(z_j = c) P\left(\sum_{k=0}^m x_k \equiv 0 \pmod{3} \mid z_1 = \dots = z_m = c\right) \right) \quad (60)$$

$$= \sum_{c=0}^2 C_c^m P\left(\sum_{k=0}^m x_k \equiv 0 \pmod{3} \mid z_1 = \dots = z_m = c\right). \quad (61)$$

(iii) Simplify the expression.

$$P\left(\sum_{k=0}^m x_k \equiv 0 \pmod{3} \mid z_1 = \dots = z_m = c\right) \quad (62)$$

$$= \sum_{t_0=0}^2 \left[ P(x_0 = t_0) \sum_{\mathbf{t} \in \mathbb{Z}_3^m} \delta_0\left(\sum_{j=0}^m t_j\right) \prod_{i=1}^m P(x_i = t_i \mid z_i = c) \right], \quad (63)$$

where  $\mathbf{t} = (t_1, \dots, t_m)$  and

$$\delta_0\left(\sum_{j=0}^m t_j\right) = \frac{1}{3} \sum_{k=0}^2 \omega^k \sum_{j=0}^m t_j = \frac{1}{3} \sum_{k=0}^2 \prod_{j=0}^m \omega^{k \cdot t_j}. \quad (64)$$

Then

$$P_{\text{succ}} = \sum_{c=0}^2 C_c^m P\left(\sum_{k=0}^m x_k \equiv 0 \pmod{3} \mid z_1 = \dots = z_m = c\right) \quad (65)$$

$$= \sum_{c=0}^2 C_c^m \sum_{t_0=0}^2 \left[ P(x_0 = t_0) \sum_{\mathbf{t} \in \mathbb{Z}_3^m} \left( \frac{1}{3} \sum_{k=0}^2 \prod_{j=0}^m \omega^{k t_j} \prod_{i=1}^m P(x_i = t_i \mid z_i = c) \right) \right] \quad (66)$$

$$= \frac{1}{3} \sum_{c=0}^2 C_c^m \sum_{k=0}^2 \sum_{t_0=0}^2 P(x_0 = t_0) \omega^{k t_0} \sum_{\mathbf{t} \in \mathbb{Z}_3^m} \left[ \prod_{i=1}^m \omega^{k t_i} P(x_i = t_i \mid z_i = c) \right], \quad (67)$$

where the inner sum simplifies as

$$\sum_{\mathbf{t} \in \mathbb{Z}_3^m} \left[ \prod_{i=1}^m \omega^{k t_i} P(x_i = t_i \mid z_i = c) \right] = \prod_{i=1}^m \sum_{t_i=0}^2 [\omega^{k t_i} P(x_i = t_i \mid z_i = c)] \quad (68)$$

$$= \left[ \sum_{t=0}^2 \omega^{k t} P(x = t \mid z = c) \right]^m. \quad (69)$$

For a random variable  $Y$  taking values in  $\{0, 1, 2\}$ , the modulo-3 characteristic function is defined as

$$\phi_Y(k) := \mathbb{E}(\omega^{kY}) = \sum_{y=0}^2 P(Y = y)\omega^{ky}, k \in \{0, 1, 2\}. \quad (70)$$

Then, recognizing the definitions within our equation, we obtain

$$P_{\text{succ}} = \frac{1}{3} \sum_{c=0}^2 C_c^m \sum_{k=0}^2 \phi_{x_0}(k) [\phi_{x|z=c}(k)]^m. \quad (71)$$

(iv) Calculate each part separately.

Using the specific values of  $C_c$  from (56), we evaluate the carrier conditional characteristic function,

$$\phi_{x|z=c}(k) = \frac{1}{C_c} \sum_{t=0}^2 P(c, t)\omega^{kt}. \quad (72)$$

Evaluating this for each  $c \in \{0, 1, 2\}$  yields

$$\phi_{x|z=c}(k) = \begin{cases} 1, & k = 0 \text{ (for all } c), \\ \frac{9p-1}{2(3p+1)}, & k = 1, 2 \text{ and } c = 0, \\ 0, & k = 1, 2 \text{ and } c \in \{1, 2\}. \end{cases} \quad (73)$$

Next, we evaluate the characteristic function  $\phi_{x_0}(k)$  of the shared state  $x_0$ . We define the probabilities  $R_i$  for  $i \in \{0, 1, 2\}$  as

$$R_i := P(x_0 = i) = \sum_{j=0}^2 r_{ij}. \quad (74)$$

The characteristic function is then directly expressed as

$$\phi_{x_0}(k) = \sum_{i=0}^2 R_i \omega^{ki}. \quad (75)$$

Evaluating (75) at  $k = 0$  trivially yields the normalization condition  $\phi_{x_0}(0) = \sum_{i=0}^2 R_i = 1$ . For the non-trivial modes  $k \in \{1, 2\}$ , we algebraically decouple the sum into its symmetric and antisymmetric components. Expanding the characteristic functions yields

$$\phi_{x_0}(1) = R_0 + \frac{1}{2}(\omega + \omega^2)(R_1 + R_2) + \frac{1}{2}(\omega - \omega^2)(R_1 - R_2), \quad (76)$$

$$\phi_{x_0}(2) = R_0 + \frac{1}{2}(\omega + \omega^2)(R_1 + R_2) - \frac{1}{2}(\omega - \omega^2)(R_1 - R_2). \quad (77)$$

This explicit decomposition clearly demonstrates that  $\phi_{x_0}(1)$  and  $\phi_{x_0}(2)$  are complex conjugates, where the term proportional to  $(\omega - \omega^2)$  constitutes the pure imaginary component.

When evaluating the overall success probability  $P_{\text{succ}}$ , the pure imaginary components proportional to  $(\omega - \omega^2)$  yield no net contribution. They either vanish upon multiplication (since  $\phi_{x|z=c}(k) = 0$  for  $c \neq 0$ ) or cancel perfectly in pairs due to the symmetry of the carrier characteristic function,  $\phi_{x|z=0}(1) = \phi_{x|z=0}(2)$ . By retaining only the effective real part and applying the root identity  $\omega + \omega^2 = -1$  alongside the probability normalization  $\sum_i R_i = 1$ , the characteristic function directly simplifies to

$$\phi_{x_0}(k) = \begin{cases} 1, & k = 0, \\ \frac{3R_0 - 1}{2}, & k = 1, 2. \end{cases} \quad (78)$$

(v) Calculate  $P_{\text{succ}}$ .

Substituting the previously derived characteristic functions into the expression for  $P_{\text{succ}}$ , we evaluate the sum to obtain

$$P_{\text{succ}} = \frac{1}{3} \left( \frac{3p+1}{4} \right)^m + \frac{3R_0 - 1}{3} \left( \frac{9p-1}{8} \right)^m + \frac{2}{3} \left( \frac{3(1-p)}{8} \right)^m. \quad (79)$$

To render the subsequent analysis more readable, we introduce three auxiliary exponential decay parameters:

$$A_m := \left( \frac{3p+1}{4} \right)^m, \quad B_m := \left( \frac{9p-1}{8} \right)^m, \quad C_m := \left( \frac{3(1-p)}{8} \right)^m. \quad (80)$$

The success probability then takes the compact form

$$P_{\text{succ}} = \frac{1}{3} [A_m + (3R_0 - 1)B_m + 2C_m]. \quad (81)$$

To determine the output Bell label  $(s, t)$ , we introduce indicator functions for the measurement outcomes. For the bit-flip label  $s = i$ , we define

$$\delta(s = i) := \delta_0(i - x_0) = \frac{1}{3} \sum_{k=0}^2 \omega^{k(i-x_0)}. \quad (82)$$

According to Lemma 4, the phase-flip label satisfies  $t \equiv z_0 - z_1 \pmod{3}$ . Accordingly, its indicator is defined as

$$\delta(t = j) := \delta_0(j - z_0 + z_1) = \frac{1}{3} \sum_{k=0}^2 \omega^{k(j-z_0+z_1)}. \quad (83)$$



The joint Bell indicator factors as

$$\delta_{ij} := \mathbf{1}_{\text{succ}} \delta(s = i) \delta(t = j), \quad (84)$$

yielding the conditional probability  $q'_{st} = \mathbb{E}[\delta_{st}] / P_{\text{succ}}$ .

Our primary objective is to evaluate  $q'_{00}$  and establish that  $q'_{00} \rightarrow 1$  in the asymptotic limit. Other required conditional probabilities  $q'_{st}$  will be computed as necessary to facilitate this proof.

By substituting the explicit forms of the indicators into (84), the joint indicator for the target outcome  $(s, t) = (0, 0)$  expands as

$$\delta_{00} = \underbrace{\left( \prod_{i=1}^{m-1} \delta_0(z_i - z_m) \right)}_{\mathbf{1}_{\text{succ}}} \delta_0 \left( \sum_{k=0}^m x_k \right) \underbrace{\delta_0(x_0)}_{s=0} \underbrace{\delta_0(z_0 - z_1)}_{t=0}. \quad (85)$$

The target conditions  $s = 0$  and  $t = 0$  deterministically enforce  $x_0 = 0$  and  $z_0 = z_1$ , respectively. Absorbing these constraints into the success indicator  $\mathbf{1}_{\text{succ}}$  simplifies the expression to

$$\delta_{00} = \left( \prod_{i=0}^{m-1} \delta_0(z_i - z_m) \right) \delta_0 \left( \sum_{k=1}^m x_k \right) \delta_0(x_0). \quad (86)$$

Consequently, the joint indicator  $\delta_{00}$  is non-vanishing if and only if all particles (index 0 for the shared state and indices  $1, \dots, m$  for the carriers) simultaneously satisfy the following constraints:

$$\begin{cases} z_0 = z_1 = \dots = z_m = \gamma, & \gamma \in \{0, 1, 2\}, \\ x_0 = 0 \quad \text{and} \quad \sum_{k=1}^m x_k \equiv 0 \pmod{3}. \end{cases} \quad (87)$$

Next, we decompose the expectation value  $\mathbb{E}[\delta_{00}]$  by conditioning on the mutually exclusive values of the common  $Z$ -error,  $\gamma \in \{0, 1, 2\}$ . Since the shared state and the carriers are independent after preprocessing, the joint probability factorizes. Letting  $r_{ij} := P_0(i, j)$  denote the initial error probabilities of the shared state, the expectation expands as

$$\begin{aligned} \mathbb{E}[\delta_{00}] &= \sum_{\gamma=0}^2 P_0(0, \gamma) P \left( \sum_{k=1}^m x_k \equiv 0 \pmod{3} \mid \forall k, z_k = \gamma \right) P(\forall k, z_k = \gamma) \\ &= \frac{1}{3} \sum_{\gamma=0}^2 r_{0\gamma} C_\gamma^m \sum_{k=0}^2 [\phi_{x|z=\gamma}(k)]^m \\ &= \frac{r_{00}}{3} (A_m + 2B_m) + \frac{r_{01} + r_{02}}{3} C_m. \end{aligned} \quad (88)$$

Dividing by  $P_{\text{succ}}$  yields the normalized conditional probability,

$$q'_{00} = \frac{1}{3P_{\text{succ}}} [r_{00}(A_m + 2B_m) + (r_{01} + r_{02})C_m]. \quad (89)$$

For the outcomes  $q'_{01}$  and  $q'_{02}$ , the target bit-flip label  $s = 0$  remains fixed, but the phase-flip target  $t = j$  (where  $j \in \{1, 2\}$ ) modifies the constraint to  $z_0 - \gamma \equiv j \pmod{3}$ . Physically, this simply induces a cyclic permutation of the shared state's  $Z$ -error indices  $r_{0\gamma}$ . Leaving the rest of the derivation structurally identical, we immediately obtain

$$q'_{01} = \frac{1}{3P_{\text{succ}}} [r_{01}(A_m + 2B_m) + (r_{02} + r_{00})C_m], \quad (90)$$

$$q'_{02} = \frac{1}{3P_{\text{succ}}} [r_{02}(A_m + 2B_m) + (r_{00} + r_{01})C_m]. \quad (91)$$

When evaluating the cases where  $s \neq 0$ , the  $X$ -error constraint shifts. For instance, fixing  $s = 1$  requires  $x_0 = 1$ , which modifies the carrier sum condition to  $\sum_{k=1}^m x_k \equiv -1 \pmod{3}$ . The joint indicator  $\delta_{10}$  becomes

$$\delta_{10} = \left( \prod_{i=0}^{m-1} \delta_0(z_i - z_m) \right) \delta_0 \left( \sum_{k=1}^m x_k + 1 \right) \delta_0(x_0 - 1). \quad (92)$$

Expanding the indicator for the carrier sum,  $\delta_0(\sum_{k=1}^m x_k + 1)$ , explicitly factors out an extra phase  $\omega^k$  due to the constant offset  $+1$ . Since the characteristic function is symmetric,  $\phi_{x|z=0}(1) = \phi_{x|z=0}(2)$ , applying the identity  $\omega + \omega^2 = -1$  precisely flips the sign of the  $B_m$  term in the expectation,

$$\begin{aligned} \mathbb{E}[\delta_{10}] &= \frac{1}{3} \sum_{\gamma=0}^2 r_{1\gamma} C_\gamma^m \sum_{k=0}^2 \omega^k [\phi_{x|z=\gamma}(k)]^m \\ &= \frac{r_{10}}{3} (A_m - B_m) + \frac{r_{11} + r_{12}}{3} C_m. \end{aligned} \quad (93)$$

Normalizing yields  $q'_{10}$ . Applying the same cyclic permutation argument for  $t \in \{1, 2\}$  provides the complete set for  $s = 1$ ,

$$q'_{10} = \frac{1}{3P_{\text{succ}}} [r_{10}(A_m - B_m) + (r_{11} + r_{12})C_m], \quad (94)$$

$$q'_{11} = \frac{1}{3P_{\text{succ}}} [r_{11}(A_m - B_m) + (r_{12} + r_{10})C_m], \quad (95)$$

$$q'_{12} = \frac{1}{3P_{\text{succ}}} [r_{12}(A_m - B_m) + (r_{10} + r_{11})C_m]. \quad (96)$$

Finally, the analysis for  $s = 2$  proceeds in complete analogy. Fixing  $s = 2$  requires  $x_0 = 2$ , which shifts the carrier sum condition to  $\sum_{k=1}^m x_k \equiv 1 \pmod{3}$ . Expanding the corresponding indicator yields a conjugate phase factor  $\omega^{-k}$  (or equivalently  $\omega^{2k}$ ). Due to the symmetry of the characteristic function, this phase factor again evaluates to  $\omega^2 + \omega = -1$ , yielding the identical  $(A_m - B_m)$  dependence. Applying the cyclic permutation of the  $Z$ -error indices  $r_{2\gamma}$  for the phase-flip target  $t \in \{0, 1, 2\}$  provides the final set of conditional probabilities,

$$q'_{20} = \frac{1}{3P_{\text{succ}}} [r_{20}(A_m - B_m) + (r_{21} + r_{22})C_m], \quad (97)$$

$$q'_{21} = \frac{1}{3P_{\text{succ}}} [r_{21}(A_m - B_m) + (r_{22} + r_{20})C_m], \quad (98)$$

$$q'_{22} = \frac{1}{3P_{\text{succ}}} [r_{22}(A_m - B_m) + (r_{20} + r_{21})C_m]. \quad (99)$$

For convenience, we summarize the conditional probabilities  $q'_{st}$  derived above. Recognizing the cyclic permutation in the phase-flip index  $t$ , the nine expressions can be compactly written as a generalized formula,

$$q'_{st} = \frac{1}{3P_{\text{succ}}} \begin{cases} r_{st}(A_m + 2B_m) + (r_{s,t\oplus 1} + r_{s,t\oplus 2})C_m, & s = 0, \\ r_{st}(A_m - B_m) + (r_{s,t\oplus 1} + r_{s,t\oplus 2})C_m, & s \in \{1, 2\}, \end{cases} \quad (100)$$

where the addition in the second subscript is performed modulo 3 ( $\oplus$ ), and the parameters  $A_m, B_m, C_m$ , and  $P_{\text{succ}}$  are given by (80) and (81). One can readily verify that these probabilities are properly normalized,  $\sum_{s,t=0}^2 q'_{st} = 1$ .

To investigate whether the target state probability  $q'_{00}$  asymptotically approaches unity as  $m$  increases, we treat the transformation as a discrete dynamical map. By substituting the shared state's initial error probabilities  $r_{ij}$  with the iterative parameters  $q_{ij}$  according to the permutation rules in (43), the nine recursion relations can be compactly grouped by the output bit-flip index  $s$  and expressed in matrix form. Defining the mapped input state vectors as

$$\mathbf{v}^{(0)} = (q_{00}, q_{21}, q_{22})^T, \quad \mathbf{v}^{(1)} = (q_{10}, q_{11}, q_{12})^T, \quad \mathbf{v}^{(2)} = (q_{20}, q_{01}, q_{02})^T, \quad (101)$$

the updated probability vectors  $\mathbf{q}'^{(s)} = (q'_{s0}, q'_{s1}, q'_{s2})^T$  are given by

$$\mathbf{q}'^{(s)} = \frac{1}{3P_{\text{succ}}} \begin{pmatrix} \alpha_s & C_m & C_m \\ C_m & \alpha_s & C_m \\ C_m & C_m & \alpha_s \end{pmatrix} \mathbf{v}^{(s)}, \quad (102)$$

where the diagonal parameter  $\alpha_s$  is determined by the target subspace, defined as

$$\alpha_s = \begin{cases} A_m + 2B_m, & s = 0, \\ A_m - B_m, & s \in \{1, 2\}. \end{cases} \quad (103)$$

We determine the steady-state behavior by imposing the fixed-point condition  $\mathbf{q}' = \mathbf{q}$  and analyzing the asymptotic limit  $m \rightarrow \infty$ .

We first eliminate the non-target subspaces sequentially. Let  $R_s = \sum_{t=0}^2 q_{st}$  denote the marginal probability for subspace  $s$ . Summing the three fixed-point equations for the non-target subspace  $s = 1$  in (102) yields

$$R_1 = \frac{R_1}{3P_{\text{succ}}} [A_m - B_m + 2C_m]. \quad (104)$$

This equation admits only two solutions, requiring  $R_1 = 0$  or the bracketed term equals  $3P_{\text{succ}}$ . Assuming the latter and substituting (81) for  $P_{\text{succ}}$ , we

obtain  $3R_0B_m = 0$ , which implies  $R_0 = 0$ . However,  $R_0 = 0$  corresponds to a completely mixed final state with zero target fidelity, a physically irrelevant solution for entanglement purification. Therefore, the only valid physical solution is  $R_1 = 0$ .

With  $R_1 = 0$ , probability conservation  $\sum_{i=0}^2 R_i = 1$  enforces the constraint

$$R_0 + R_2 = 1. \quad (105)$$

Next, we apply the fixed-point condition  $q'_{00} = q_{00}$  to the general mapping in (100). Substituting  $r_{01} + r_{02} = R_0 - q_{00}$ , the steady-state equation for  $q_{00}$  becomes

$$3P_{\text{succ}}q_{00} = q_{00}(A_m + 2B_m) + (R_0 - q_{00})C_m. \quad (106)$$

Inserting the explicit expression for  $P_{\text{succ}}$  and regrouping terms algebraically, we arrive at

$$3q_{00}(R_0 - 1)B_m = (R_0 - 3q_{00})C_m. \quad (107)$$

In the working regime  $p > 1/3$ , the decay parameters satisfy the strict hierarchy  $B_m \gg C_m$  for sufficiently large  $m$ . Dividing both sides by  $B_m$  and taking the limit  $m \rightarrow \infty$  gives  $C_m/B_m \rightarrow 0$ , reducing the equation to  $3q_{00}(R_0 - 1) = 0$ . Since  $q_{00}$  must be non-zero for successful purification, it follows that  $R_0 \rightarrow 1$ . Equation (105) then immediately implies  $R_2 \rightarrow 0$ .

Since all probabilities are non-negative,  $R_2 \rightarrow 0$  requires  $q_{20}, q_{21}, q_{22} \rightarrow 0$ , while  $R_0 \rightarrow 1$  requires  $q_{01}, q_{02} \rightarrow 0$ .

Finally, to eliminate the remaining cross terms  $q_{21}$  and  $q_{22}$  that map into the target subspace, we extract the fixed-point equation for  $q_{01}$  from the matrix map in (102) for the  $s = 0$  subspace:

$$q_{01} = \frac{1}{3P_{\text{succ}}} [q_{21}(A_m + 2B_m) + (q_{22} + q_{00})C_m]. \quad (108)$$

We have already established that  $q_{01} \rightarrow 0$ . In the large- $m$  limit,  $A_m$  is the strictly dominant term ( $A_m \gg B_m \gg C_m$ ). Multiplying both sides by  $3P_{\text{succ}}$ , dividing by  $A_m$ , and taking  $m \rightarrow \infty$  retains only the leading-order contribution:

$$q_{21} \cdot 1 + (q_{22} + q_{00}) \cdot 0 = 0 \quad \Rightarrow \quad q_{21} \rightarrow 0. \quad (109)$$

By symmetry, an identical analysis of  $q_{02}$  yields  $q_{22} \rightarrow 0$ .

With all non-target components eliminated, normalization guarantees

$$q_{00} \rightarrow 1. \quad (110)$$

## Appendix B Proof of Theorem 8

Consider an arbitrary three-dimensional general Pauli channel, defined in (3), with an initial error distribution  $\{p_{nm}\}$ . According to the Horodecki reduction criterion, if the initial fidelity satisfies  $p_{00} > 1/3$ , the resulting Bell-diagonal

shared state necessarily violates the reduction criterion. Hence, it is an absolute NPT state and is theoretically distillable.

We will prove that after  $n$  rounds of the mCAEPP with alternating bases, when the number of rounds  $n \rightarrow \infty$  and the number of carriers  $m$  per round is sufficiently large, the fidelity of the shared state for this general Pauli channel converges constructively to 1.

The complete single-round iteration of the  $m$ -carrier-assisted alternating-basis entanglement purification protocol (mCAEPP) proceeds as follows.

First, a one-time MUB-based adaptive preprocessing is performed, executed only once before the first iteration.

Next, the protocol executes a multi-carrier check in the  $Z$  basis. By introducing  $m$  independent and identically distributed auxiliary carriers, applying bilateral SUM gates, and subsequently measuring the carriers in the  $Z$  basis, the protocol extracts the error syndrome. This post-selection effectively suppresses shift errors.

Subsequently, a bilateral three-dimensional Hadamard transform  $H_3 \otimes H_3$  is applied, realizing a phase-space permutation between  $X$  and  $Z$ .

Finally, the multi-carrier check from the second step is repeated to suppress bit-flip errors in the original coordinate system, completing the single-round iteration.

For the shared state at the  $n$ -th iteration round, characterized by the error probability distribution  $\{p_{xz}^{(n)}\}$ , we introduce the core dynamical parameters to systematically analyze the decoupled suppression of errors. Specifically, the marginal probability for a given shift error  $x$  is defined as

$$u_x^{(n)} = \sum_{z=0}^2 p_{xz}^{(n)}. \quad (111)$$

Correspondingly, the marginal probability for a given phase error  $z$  is defined as

$$v_z^{(n)} = \sum_{x=0}^2 p_{xz}^{(n)}. \quad (112)$$

The relative error coefficients quantify the contamination ratio of each non-trivial error branch with respect to the target state, defined as

$$\epsilon_{xz}^{(n)} = \frac{p_{xz}^{(n)}}{p_{00}^{(n)}} \quad (113)$$

for all  $(x, z) \neq (0, 0)$ , with the coefficient of the target state itself fixed as

$$\epsilon_{00}^{(n)} \equiv 1. \quad (114)$$

Combined with the probability normalization condition, this definition directly yields the relation

$$p_{00}^{(n)} = \frac{1}{1 + \sum_{(x,z) \neq (0,0)} \epsilon_{xz}^{(n)}}. \quad (115)$$

The proof of fidelity convergence is therefore equivalent to proving

$$\lim_{n \rightarrow \infty} \epsilon_{xz}^{(n)} = 0 \quad (116)$$

for all nontrivial error terms with  $(x, z) \neq (0, 0)$ .

We adopt the half-iteration notation  $n + 0.5$  to label the intermediate state within the  $n$ -th iteration round, which is obtained after the completion of the  $Z$ -basis multi-carrier parity check and before the phase space rotation transformation. All corresponding physical quantities for this intermediate state are marked with the superscript  $(n + 0.5)$ .

The core prerequisite for the purification iteration is establishing a ‘spectral dominance condition’. Specifically, one must apply lossless local operations to actively enforce absolute dominance of the marginal error probability along a single axis. This dominance provides the crucial mathematical foundation for the subsequent suppression of exponential errors. This protocol provides a deterministic and lossless preprocessing scheme based on the algebraic–geometric structure of a three-dimensional discrete phase space and mutually unbiased bases (MUBs).

The discrete phase space for the prime dimension  $d = 3$  is defined as  $\mathbb{Z}_3 \times \mathbb{Z}_3$ , containing 9 lattice points. Each lattice point  $(n, m)$  uniquely corresponds to a generalized Pauli operator  $X^n Z^m$ , and simultaneously uniquely corresponds to the weight  $p_{nm}$  of the Bell-diagonal state. The origin  $(0, 0)$  corresponds to the weight  $p_{00}$  of the target state.

In the prime dimension  $d$ , the maximum number of pairwise mutually unbiased bases is  $d + 1 = 4$ . Each MUB uniquely corresponds to a striation in the phase space: a set of  $d$  parallel lines, each containing  $d$  lattice points, that partition the entire  $d^2$  lattice points without overlap. The line passing through the origin  $(0, 0)$  in each striation exactly corresponds to the error symmetry direction of that MUB. The origin-passing lines corresponding to the 4 MUBs are

$$\begin{cases} L_1 = p_{00} + p_{10} + p_{20} & (m = 0, Z \text{ basis}), \\ L_2 = p_{00} + p_{01} + p_{02} & (n = 0, X \text{ basis}), \\ L_3 = p_{00} + p_{11} + p_{22} & (m = n, XZ \text{ basis}), \\ L_4 = p_{00} + p_{12} + p_{21} & (m = 2n, XZ^2 \text{ basis}). \end{cases} \quad (117)$$

From the above construction, the 8 non-origin lattice points belong to exactly one origin-passing MUB line. Thus, the sum of weights of the 4 lines satisfies the identity

$$\sum_{i=1}^4 L_i = 3p_{00} + 1 > 2. \quad (118)$$

By the pigeonhole principle, there must exist at least one origin-passing MUB line with weight sum

$$L_{\max} = \max\{L_1, L_2, L_3, L_4\} > 1/2. \quad (119)$$

The three-dimension Clifford group can deterministically map any two sets of MUBs via local unitary operations, while preserving the Bell-diagonal form of the state and the initial fidelity  $p_{00}$ . After synchronizing channel tomography results via classical communication, Alice and Bob apply bilateral local Clifford operations to rotate the MUB line with  $L_{\max}$  to the line  $L_1$  corresponding to the  $Z$  basis.

This rotation aligns the dominant error symmetry direction with the computational basis, and the preprocessed initial state at  $n = 0$  satisfies  $u_0^{(0)} = L_{\max} > 1/2$ . Combined with the normalization condition of marginal probabilities, this directly enforces  $\max\{u_1^{(0)}, u_2^{(0)}\} < 1/2$ , which rigorously establishes the spectral dominance condition required for iterative purification.

Following the preprocessing, the protocol executes a sequence of continuous  $Z$ -basis multi-carrier parity checks to suppress shift errors. Alice and Bob repeat these  $Z$ -basis checks over  $k$  consecutive rounds. Because this parity check selectively filters shift errors (the  $x$  index) while leaving the pure phase errors (the  $z$  index) invariant, the relative error coefficients for any branch with  $x \neq 0$  evolve as

$$\epsilon_{xz}^{(k)} = \epsilon_{xz}^{(0)} \left( \frac{u_x^{(0)}}{u_0^{(0)}} \right)^{km}. \quad (120)$$

Because  $u_0^{(0)} > u_x^{(0)}$  for all  $x \neq 0$ , the decay factor is strictly less than unity. As  $k \rightarrow \infty$  (or for sufficiently large  $m$ ),  $\epsilon_{xz}^{(k)} \rightarrow 0$ . This deterministically projects the state into the  $x = 0$  subspace, spanned exclusively by the target state  $|\Phi^{0,0}\rangle$  and pure phase errors  $|\Phi^{0,1}\rangle, |\Phi^{0,2}\rangle$ .

To purify these residual errors, a bilateral Hadamard transform  $H_3 \otimes H_3$  is applied. This maps  $X^0 Z^z \rightarrow X^z Z^0$ , converting phase errors into shift errors ( $p_{0z} \rightarrow p_{z0}$ ). Resuming continuous parity checks, the newly formed shift errors evolve from the intermediate state ( $0'$ ) over  $k'$  rounds as

$$\epsilon_{z0}^{(k')} = \epsilon_{z0}^{(0')} \left( \frac{p_{z0}}{p_{00}} \right)^{k'm}. \quad (121)$$

For any distillable state ( $p_{00} > 1/3$ ), the target state possesses the maximal single-state weight, rigorously ensuring  $p_{00} > p_{01}$  and  $p_{00} > p_{02}$ . Consequently,  $p_{z0}/p_{00} < 1$ , yielding  $\lim_{k' \rightarrow \infty} \epsilon_{z0}^{(k')} = 0$  for all  $z \neq 0$ .

By decoupling the suppression of shift and phase errors, this asymmetric strategy eradicates all non-trivial errors, driving the fidelity unconditionally to 1.

## References

- [1] Charles H. Bennett, Gilles Brassard, Claude Crépeau, Richard Jozsa, Asher Peres, and William K. Wootters. Teleporting an unknown quantum state via dual classical and einstein-podolsky-rosen channels. *Phys. Rev. Lett.*, 70:1895–1899, Mar 1993.

- [2] Reinhard F. Werner. Quantum states with einstein-podolsky-rosen correlations admitting a hidden-variable model. *Physical Review A*, 40:4277–4281, Oct 1989.
- [3] A. Peres. Separability criterion for density matrices. *Phys. Rev. Lett.*, 77:1413, 1996.
- [4] M. Horodecki, P. Horodecki, and R. Horodecki. Separability of mixed states: necessary and sufficient conditions. *Physics Letters A*, 223:1–8, February 1996.
- [5] Michal Horodecki and Pawel Horodecki. Reduction criterion of separability and limits for a class of protocols of entanglement distillation. *Physics*, 59(59):4206–4216, 1997.
- [6] Micha Horodecki, Pawe Horodecki, and Ryszard Horodecki. Inseparable two spin- density matrices can be distilled to a singlet form. *Physical Review Letters*, 78(4):574–577, 1997.
- [7] Michal Horodecki, Pawel Horodecki, and Ryszard Horodecki. Mixed-state entanglement and distillation: Is there a bound a entanglement in nature? *Phys. Rev. Lett.*, 80:5239–5242, 1998.
- [8] Pawel Horodecki, Lukasz Rudnicki, and Karol Zyczkowski. Five open problems in quantum information, 2020. arXiv:2002.03233v1.
- [9] David P. Divincenzo, Peter W. Shor, John A. Smolin, Barbara M. Terhal, and Ashish V. Thapliyal. Evidence for bound entangled states with negative partial transpose. *Physical Review A*, 61(6):062312, 2000.
- [10] John Watrous. Many copies may be required for entanglement distillation. *Phys. Rev. Lett.*, 93:010502, 2004.
- [11] Reinaldo O. Vianna and Andrew C. Doherty. Distillability of werner states using entanglement witnesses and robust semidefinite programs. *Phys. Rev. A*, 74:052306, 2006.
- [12] Lin Chen, Wai Shing Tang, and Yu Yang. Generalized choi states and 2-distillability of quantum states. *Quantum Information Processing*, 17(5):110, 2018.
- [13] Pawel Horodecki, John A. Smolin, Barbara M. Terhal, and Ashish V. Thapliyal. Rank two bound entangled states do not exist. 1999.
- [14] Lin, Chen, Yi-Xin, and Chen. Rank-three bipartite entangled states are distillable. *Physical Review A*, 78(2):22318–22318, 2008.
- [15] Lin Chen and Dragomir Z Djokovic. Distillability of non-positive-partial-transpose bipartite quantum states of rank four. *Phys. Rev. A*, 94:052318, Nov 2016.



- [16] Lin Chen and Dragomir Z Djokovic. Distillability and ppt entanglement of low-rank quantum states. *Journal of Physics A: Mathematical and Theoretical*, 44(28):285303, 2011.
- [17] E. M. Rains. Bound on distillable entanglement. *Phys. Rev. A*, 60:179, 1999.
- [18] E. M. Rains. A semidefinite program for distillable entanglement. *IEEE Trans. Inform. Theory*, 47:2921, 2001.
- [19] I. Devetak and A. Winter. Distillation of secret key and entanglement from quantum states. *Proc. R. Soc. A*, 461:207, 2005.
- [20] P. G. Kwiat, S Barraza-Lopez, A Stefanov, and N Gisin. Experimental entanglement distillation and 'hidden' non-locality. *Nature*, 409(6823):1014–7, 2001.
- [21] Lin Chen and Masahito Hayashi. Nondistillable entanglement guarantees distillable entanglement. *International Journal of Modern Physics B*, 26(27n28):1243008, 2012.
- [22] Manuel Erhard, Mario Krenn, and Anton Zeilinger. Advances in high dimensional quantum entanglement. *Nature Reviews Physics*, 2019.
- [23] Yi Han Luo, Han Sen Zhong, Manuel Erhard, Xi Lin Wang, Li Chao Peng, Mario Krenn, Xiao Jiang, Li Li, Nai Le Liu, and Chao Yang Lu. Quantum teleportation in high dimensions. *Phys. Rev. Lett.*, 123(7):070505.1–040505.6, 2019.
- [24] Zhi Feng Liu, Zhi Cheng Ren, Pei Wan, Wen Zheng Zhu, Zi Mo Cheng, Jing Wang, Yu Peng Shi, Han Bing Xi, Marcus Huber, and Nicolai Friis. Heralded high-dimensional photon–photon quantum gate. *Nature Photonics*, 20(4):460–467, 2026.
- [25] Allen Zang, Xinan Chen, Eric Chitambar, Martin Suchara, and Tian Zhong. No-go theorems for universal entanglement purification. *Phys. Rev. Lett.*, 134(19):190803, 2025.
- [26] Ludovico Lami, Bartosz Regula, and Alexander Streltsov. No-go theorem for entanglement distillation using catalysis. *Physical Review A*, 109(5):6, 2024.
- [27] Ohad Lib, Shuheng Liu, Ronen Shekel, Qiongyi He, Marcus Huber, Yaron Bromberg, and Giuseppe Vitagliano. Experimental certification of high-dimensional entanglement with randomized measurements. *Phys. Rev. Lett.*, 134(21):210202, 2025.
- [28] Simon Morelli, Marcus Huber, and Armin Tavakoli. Resource-efficient high-dimensional entanglement detection via symmetric projections. *Phys. Rev. Lett.*, 131(17):170201.1–170201.8, 2023.

- [29] Xiao Min Hu, Chao Zhang, Yu Guo, Fang Xiang Wang, Wen Bo Xing, Cen Xiao Huang, Bi Heng Liu, Yun Feng Huang, Chuan Feng Li, and Guang Can Guo. Pathways for entanglement-based quantum communication in the face of high noise. *Phys. Rev. Lett.*, (11), 2021.
- [30] Peter W. Shor, Michael Horodecki, and Mary Beth Ruskai. Entanglement breaking channels. *Reviews in Mathematical Physics*, 2003.